Environmental Science Nano

Co-effects of UV/H_2O_2 and Natural Organic Matter on the Surface Chemistry of Cerium Oxide Nanoparticles

Journal:	*Environmental Science: Nano*
Manuscript ID	EN-ART-04-2018-000435.R1
Article Type:	Paper
Date Submitted by the Author:	02-Jul-2018

Complete List of Authors:	Wu, Xuanhao; Washington University, Department of Energy, Environmental and Chemical Engineering Neil, Chelsea; Washington University, Department of Energy, Environmental and Chemical Engineering Kim, Doyoon; Washington University, Department of Energy, Environmental and Chemical Engineering Jung, Haesung; Washington University, Department of Energy, Environmental and Chemical Engineering Jun, Young-Shin; Washington University, Department of Energy, Environmental and Chemical Engineering

Environmental significance

Cerium oxide nanoparticles (CeO_2 NPs) are important engineered nanomaterials (ENMs) that are widely used as catalysts in industrial applications, which lead to their notable presence in both natural and engineered water systems. In wastewater treatment plants (WWTPs), CeO_2 NPs can remain colloidally stable and be released in the secondary effluents. After their entrance into tertiary treatment processes, such as advanced oxidation processes (AOPs), it is important to know how the reactive oxygen species (ROS) generated will alter the colloidal stability, aggregation, and the surface chemistry of CeO_2 NPs, and to understand the influence of organic matter, such as natural organic matter (NOM) on the reactions between CeO_2 NPs and ROS. This study reports, for the first time, that the ROS generated during the UV/H_2O_2 (i.e., $O_2^{\cdot-}$) reaction promoted the sedimentation of CeO_2 NPs. The coating of NOM on CeO_2 NPs surface helped to stabilize CeO_2 NPs and acted as a protective layer to resist their reaction with ROS. New findings from this work provide useful insights into predicting the fate and transport of important redox-sensitive engineered nanomaterials during water treatment processes.

Co-effects of UV/H_2O_2 and Natural Organic Matter on the Surface Chemistry of Cerium Oxide Nanoparticles

Xuanhao Wu[1], Chelsea W. Neil[1], Doyoon Kim[1], Haesung Jung[1], and Young-Shin Jun[1,*]

[1]*Department of Energy, Environmental and Chemical Engineering, Washington University, St. Louis, MO 63130*

E-mail: ysjun@seas.wustl.edu

http://encl.engineering.wustl.edu/

Submitted: July 2018

Environmental Science: Nano

*To Whom Correspondence Should be Addressed

ABSTRACT

The widespread industrial applications of cerium oxide (CeO_2) nanoparticles (NPs) have increased their likelihood of entering into natural and engineered aqueous environments. This study investigates the surface chemistry changes of CeO_2 NPs at pH 5.4 in the presence of both UV/H_2O_2 and natural organic matter (NOM). This condition can be relevant to advanced oxidation processes (AOPs). The results indicated that NOM stabilized CeO_2 NPs in solution through surface complexation between the COO^- functional groups of NOM and CeO_2 surfaces, reversing the zeta potential of CeO_2 from 39.5 ± 2.7 mV to -38.3 ± 1.8 mV. Exposure to the UV/H_2O_2 treatment reduced the colloidal stability of CeO_2 NPs, increased the percentage of Ce^{3+} on the surface from 17.8% to 28.3%, and lowered the zeta potential to close to neutral (3.8 ± 3.4 mV). With UV/H_2O_2 and NOM together, NOM coated on CeO_2 NPs acted as a protective layer, making the direct reactions between reactive oxygen species (ROS) and CeO_2 and their impacts on the colloidal stability to be insignificant in a short reaction period. During the UV/H_2O_2 treatment, the adsorption of superoxide radicals ($O_2^{\cdot-}$) dominated in neutralizing the surface charge of CeO_2, leading to decreased electrostatic repulsive forces between nanoparticles and a higher extent of sedimentation. These new findings provide important implications for understanding the colloidal stability, sedimentation, and surface chemical properties of CeO_2 NPs in aqueous systems where NOM and ROS are present.

1. Introduction

Cerium oxide (CeO_2) nanoparticles (NPs) have been widely utilized as an engineered nanomaterial (ENM) in industrial applications, such as chemical mechanical polishing (CMP) processes and catalytic processes.[1] The wide applications of CeO_2 NPs have led to a higher possibility of their existence in natural and engineered water systems. An estimated 10,000 metric tons of CeO_2 NPs were produced and used in 2010 globally, of which 1,100 metric tons went through wastewater treatment plants (WWTPs).[2] In WWTPs, the majority of CeO_2 NPs can be removed by activated sludge through adsorption or aggregation.[3-6] However, a significant fraction of the total CeO_2 NPs introduced to wastewater (up to 6–11 wt%) can still remain in the secondary effluents due to the influence of surface charge and stabilizing surfactants.[3-7] The remaining CeO_2 NPs in the secondary effluents will then be released into subsequent engineered or natural water systems, in which they might form aggregates or remain colloidally stable, affecting the water quality and resulting toxicity to the biosphere.[8-10] Therefore, it is vital to improve our understanding of the fate and transport of CeO_2 NPs after their release in secondary effluents.

In addition to traditional wastewater treatment methods, advanced oxidation processes (AOPs) have been developed and utilized in last few decades to achieve tertiary treatment of contaminants.[11, 12] Thus, the CeO_2 NPs remaining in secondary effluents could enter AOPs. UV-driven AOPs, such as the UV/H_2O_2 process, are widely used due to their high removal rate of contaminants and lower cost compared with ozone (O_3) treatment.[12, 13] During UV/H_2O_2, ultraviolet radiation cleaves the O–O bond in H_2O_2 and generates hydroxyl radicals (·OH).[14] Subsequent chain reactions produce other powerful reactive oxygen species (ROS), including superoxide radicals ($O_2^{\cdot-}$).[15-17] CeO_2 NPs have been shown to be able to react with ROS, and the

scavenging effect of CeO_2 on ROS has been reported in biological systems.[18] The redox cycles between the Ce^{3+} and Ce^{4+} oxidation states allow CeO_2 NPs to react catalytically with $O_2^{\cdot-}$/·OH, mimicking the behavior of two key antioxidant enzymes, superoxide dismutase and catalase.[19-22] Interestingly, no studies have examined the chemical reactions of CeO_2 NPs under combined UV/H_2O_2 conditions, which generates $O_2^{\cdot-}$ or ·OH from H_2O_2. The effects of these two ROS in affecting the surface chemistry, colloidal stability, and aggregation of CeO_2 NPs are thus still unknown. Furthermore, a better mechanistic understanding of the relationship between the surface chemistry change and the aggregation of CeO_2 NPs is needed.

Natural organic matter (NOM), one of the major components in wastewater,[23-25] also reacts with CeO_2 NPs. Derived from the degradation of plants and microorganisms in natural systems, NOM enters into engineered water treatment processes, causing problems including unwanted disinfection byproducts and bacterial regrowth in water distribution systems.[26, 27] The humic-substances of NOM can also be produced from biological processes in WWTPs, and constitute an important fraction of the total soluble microbial products (SMPs).[28-31] NOM is a complex mixture of different organic constituents, containing carboxylic groups, phenolic groups, and aromatic structures.[32] NOM can adsorb onto nanoparticles' surfaces through various mechanisms,[33-35] altering the surface charge,[36] colloidal stability,[37-41] and hydrophobicity/hydrophilicity of NPs.[42] Previous studies have reported the stabilization of CeO_2 NPs by NOM.[43-45] The influence of NOM on the toxicity and bioaccumulation of CeO_2 NPs has also been examined recently.[46] In WWTPs, besides associating with microbial products,[3, 47] CeO_2 NPs can also form complexes with NOM. Due to NOM's notable presence in wastewater and its ability to stabilize CeO_2 NPs in an early stage of treatment processes, NOM can play an important role in controlling the fate and transport of CeO_2 NPs before their entrance into AOPs.

However, the detailed mechanism of NOM adsorption onto CeO_2 NPs surfaces and the influence of AOPs on the adsorption process have not been fully investigated.

As a major constituent of effluent organic matter (EfOM) in secondary effluents, NOM (~ 5 mg C/L) can also enter into tertiary treatment processes, including AOPs.[48, 49] During AOPs, NOM can be partially oxidized quickly,[50] leading to a decrease in its aromaticity,[51] molecular size,[52] and hydrophobicity.[53] After CeO_2 NPs-NOM complexes enter AOPs, the ROS generated could react with both CeO_2 NPs and NOM, possibly changing the NOM coating and the surface chemical properties CeO_2 NPs. The main goal of this study was to evaluate the co-effects of ROS and NOM on the colloidal stability, surface charge, and Ce^{3+}/Ce^{4+} oxidation state change of CeO_2 NPs during the UV/H_2O_2 process. Using a combination of qualitative and quantitative methods, the roles of two different ROS ($O_2^{\cdot-}$/·OH) were also elucidated. Our findings are crucial for understanding the impacts of NOM and ROS on the fate and transport of CeO_2 NPs in AOPs.

2. Experimental Section

2.1 Chemicals and materials

Reaction solutions were prepared using sodium chloride (NaCl, ACS grade, BDH, PA), hydrogen peroxide (H_2O_2, 30%, ACS grade, BDH, PA), 2-methyl-2-propanol (tertbutyl alcohol, t-ButOH, > 99.5%, Sigma Aldrich, MO), superoxide dismutase (SOD, Cu/Zn-SOD, ≥ 90%, Sigma Aldrich, MO), and ultrapure deionized (DI) water (resistivity > 18.2 MΩ-cm). To prepare CeO_2 NPs suspended solutions, purchased CeO_2 NPs (Sigma Aldrich, MO) were used to better represent commercially available engineered NP−environmental systems. CeO_2 NPs were characterized using high resolution transmission electron microscopy (HRTEM, JEOL 2100F) (Fig. S1A and S1B in ESI†) and wide angle X-ray diffraction (WAXRD) in sector 11-ID-B at the Advanced Photon Source (APS) at Argonne National Laboratory (IL, USA) (Fig. S1C†).

Suwannee River NOM (SRNOM, 2R101N, RO isolation), purchased from the International Humic Substances Society, was the NOM source. Details on the preparation of SRNOM stock solutions and the characterization of SRNOM are in the ESI (Table S1).[54] For all experiments, 10 mM of NaCl solution was added to ensure consistent ionic strength (IS). The initial pH of all solutions, 5.4 ± 0.2, was chosen for two reasons. First, this was the pH of the system after adding NaCl, thus reducing the effects of pH adjustment on the ionic strength. Second, acidic conditions (pH 3–6) are preferred in most established UV/H_2O_2 systems due to their higher efficiency in producing ROS.[55] A high intensity UVA lamp (Ultra-Violet Products Ltd., Black ray B-100A, Upland, CA) was the UV source. The irradiance spectrum of the UVA light source is provided in the ESI (Fig. S2†).

2.2 Colloidal CeO_2 NPs and aqueous chemistry measurements.

To quantify changes in the colloidal stability and the sedimentation of CeO_2 NPs, UV−Vis spectroscopy (Thermo Fisher Scientific Inc., Evolution 60S, Waltham, MA) was utilized to measure the absorbance of CeO_2 at a wavelength of 305 nm, where the absorbance is proportional to CeO_2 concentration.[56] Six different systems were tested for both light and dark conditions: CeO_2 NPs-only system (light/dark); CeO_2 NPs with 3 and 30 mM H_2O_2 (light/dark); CeO_2 NPs with NOM (light/dark); and CeO_2 NPs with 3 and 30 mM H_2O_2 with NOM (light/dark) (Table S2†). Triplicate experiments were conducted for each condition. The CeO_2 NPs-only system in the dark was called as the control system. For each reaction condition, 50 mg/L CeO_2 NP dispersions were created in 50 mL test tubes and ultrasonicated for 1 hr before reaction, using an ultrasonic bath (model no. FS6, Fisher Scientific). The H_2O_2 concentrations chosen in this study have been commonly used, both in industrial UV/H_2O_2 systems and in previous studies.[57, 58] The concentration of NOM was 3.3 ± 0.2 mg C/L, confirmed by a non-purgeable

organic carbon measurement (NPOC, Shimadzu TOC Analyzer). This concentration of NOM is in the range of NOM concentrations commonly found in wastewater effluents.[48, 49] Aliquots of CeO_2 NPs dispersions were taken from the supernatant at 0, 20, 40, 60, 80, 100, and 120 minutes during particle sedimentation experiments. Percentages of suspended CeO_2 NPs were obtained by normalization using the initial concentrations. The detailed experimental design for the UV-Vis study is available in the ESI (Fig. S2†)

Zeta potential (ζ) values of CeO_2 NPs were measured using a Zetasizer (Malvern Instruments Inc., Nano ZS, Westborough, MA) with capillary Zeta cells (DTS1070) at reaction time points of 1 hr and 2 hrs. The isoelectric point of CeO_2 NPs was measured to be around pH 6.9 (Fig. S1D and Table S3, ESI†). At our pH conditions, the unreacted CeO_2 NPs should be positively charged. To measure the hydrodynamic particle diameter of CeO_2 NPs, the Zetasizer was also used with dynamic light scattering (DLS) cells (DTS0012, Malvern Instrument Inc., MA). HRTEM was used to compare the morphology of CeO_2 NPs reacted under different conditions. The pH change during the reaction period was also monitored (Table S4, ESI†). To test CeO_2 NPs dissolution during the reactions, inductively coupled plasma optical emission spectrometry (ICP-OES) was applied. Reactions were prepared as described for sedimentation experiments. At 1 hr and 2 hrs, samples were ultracentrifuged, filtered, and acidified to be measured by ICP-OES. Detailed experimental information about the dissolution test is provide in the ESI (Table S5†). Ion chromatography (IC) was incorporated to test the decomposition of NOM during the reaction with CeO_2 and UV/H_2O_2 (Fig. S5†).

2.3 Oxidation state determination using X-ray photoelectron spectroscopy (XPS)

X-ray photoelectron spectroscopy (XPS, PHI 5000 VersaProbe II, Ulvac-PHI with monochromatic Al Kα radiation (1486.6 eV)) was utilized to quantify the oxidation states of

cerium (Ce 3d) before and after reaction with UV/H_2O_2 and NOM, and to observe the adsorption of NOM as represented by carbon (C 1s) peaks. While accurate quantitative comparison of C 1s peaks is not possible, the relative quantitative change can be determined. To prepare the samples, after 2 hrs reaction, CeO_2 NP solutions were centrifuged at 5000 rpm for 15 minutes (Centrifuge 5804, Eppendorf Inc.), and the supernatants were removed, leaving only the CeO_2 NP sediment in the test tube. The sediment was left to dry in an anaerobic chamber to prevent any further oxidation by oxygen in the air. The detailed sample preparation for XPS is available in the ESI (Fig. S2†). For XPS data analysis, the binding energies were referenced to the C 1s line at 284.8 eV. The reference binding energy peaks for Ce^{3+} are at 885.0 (v′) and 903.5 (u′) eV, and the reference peaks for Ce^{4+} are at 907.2 (u′′), 900.6 (u), 897.9 (v′′′), 888.3 (v′′), and 889.1 (v) eV.[59, 60] The XPS reference binding energies, absolute values of areas for each peak, and calculated percentages for oxidation states/bonds for Ce 3d and C 1s under different reaction conditions are provided in Tables S6 and S7. Equation 1 was used to calculate the Ce^{3+} percentage on the surface, which was the sum of the Ce^{3+} peak areas over the total area.[61, 62]

$$Ce^{3+}\% = \frac{A_{u\prime}+A_{v\prime}}{A_{u\prime\prime}+A_{u\prime}+A_u+A_{v\prime\prime\prime}+A_{v\prime\prime}+A_{v\prime}+A_v} \quad . \qquad (1)$$

2.4 NOM adsorption measurements using attenuated total reflection Fourier transform infrared (ATR-FTIR) spectroscopy and contact angle measurements

Attenuated total reflection Fourier transform infrared (ATR-FTIR; Thermo Scientific Nicolet Nexus 470 spectrometer equipped with a diamond crystal) spectroscopy was used to analyze the adsorption of NOM on the CeO_2 NPs surfaces. The sample preparation process for the ATR-FTIR was the same as that for XPS analysis (Fig. S2†). An average of 400 scans with a resolution of 4 cm^{-1} was used. To determine the change in the extent of hydrophilicity/hydrophobicity of CeO_2 NPs before and after reaction with NOM and UV/H_2O_2,

we conducted replicate contact angle measurements using CeO_2 NP-sputtered Si wafers. CeO_2 NP-sputtered Si wafers were prepared using a method introduced in our previous study.[56] Reaction solutions were prepared in the same way as for the sedimentation experiment, except that CeO_2 NP-sputtered Si wafers (5 mm × 5 mm) were put into the solutions instead of CeO_2 powders. After reaction, deionized water was dropped onto the dried wafer surface, and a contact angle analyzer (Phoenix 300, Surface Electro Optics Co. Ltd) was used to measure contact angles.

2.5 ROS scavenging experiments using UV-Vis spectroscopy and X-ray photoelectron spectroscopy (XPS)

To better understand the roles of two different ROS, the hydroxyl radical (·OH) and superoxide radical ($O_2^{\cdot-}$), in affecting the sedimentation and surface properties of CeO_2, experiments using ROS scavengers were conducted. CeO_2 NPs dispersions were prepared as described in the sedimentation experiments. Tertbutyl alcohol (t-ButOH, 0.1 M) and superoxide dismutase (SOD, 0.5 μM) were used as scavengers of ·OH and $O_2^{\cdot-}$, respectively, based on equations 2–4.[63, 64]

$$(CH_3)_3COH + \cdot OH \rightarrow \cdot CH_2(CH_3)_2COH + H_2O \quad (2)$$

$$Cu^{2+} - SOD + O_2^{\cdot-} \rightarrow Cu^{+} - SOD + O_2 \quad (3)$$

$$Cu^{+} - SOD + O_2^{\cdot-} + 2H^{+} \rightarrow Cu^{2+} - SOD + H_2O_2 \quad (4)$$

Once the samples were reacted in the presence of the scavengers, UV−Vis spectroscopy was utilized to measure the absorbance of CeO_2 NPs at 305 nm. Then, X-ray photoelectron spectroscopy (XPS) was used for characterizing surface oxygen species on the CeO_2 NPs surface in the presence of different ROS.

3. Results and Discussion

3.1 Effects of UV/H_2O_2 and NOM on the colloidal stability of CeO_2 NPs

The colloidal stability of CeO_2 NPs in the presence of UV/H_2O_2 decreased significantly (Fig. 1A). Specifically, UV-Vis spectrometer results showed that, after 2 hrs, the concentration of CeO_2 NPs in the supernatant was much lower with UV and H_2O_2, than the control group, which contained only CeO_2 NPs. This indicates that UV/H_2O_2 exposure decreased the colloidal stability of CeO_2 NPs. For example, 76% of the initial CeO_2 NPs remained in the supernatant in the control group after 2 hrs, while only 24% of the initial CeO_2 NPs remained colloidally stable in the presence of UV and 30 mM H_2O_2. In the presence of NOM, almost all the CeO_2 NPs remained colloidally stable in the supernatant, indicating that NOM stabilizes CeO_2 NPs. The difference in NP sedimentation due to the presence of UV/H_2O_2 and NOM could also be observed visually (Fig. S3†). Moreover, as shown in Fig. 1A, when UV/H_2O_2 was added together with NOM, the CeO_2 NPs remained colloidally stable during the first 40 minutes, and after that, they started to settle, with 53% of the initial CeO_2 NPs remaining colloidally stable after 2 hrs. The settlement velocity was close to that of CeO_2 NPs with UV/H_2O_2, while faster than the settlement velocity of the CeO_2 NPs only system. These observations suggest that there was reaction between CeO_2 NPs and UV/H_2O_2 after 40 minutes, but before 40 minutes, this reaction was not significant. IC results (Fig. S5†) show that NOM itself also participated in redox reactions with UV/H_2O_2 and decomposed rapidly into smaller molecules (i.e., acetate) during the first 40 minutes. Considering the results from both the UV-Vis and IC measurements, in the first 40 minutes, ROS generated from UV/H_2O_2 reacted mainly with NOM, and after that, ROS reacted with CeO_2 NPs to promote their aggregation. Thus, we infer that NOM on CeO_2

NPs acted as a protective layer, which made the reactions between CeO_2 NPs and ROS insignificant in a shorter reaction period.

To understand the effects of UV/H_2O_2 and NOM on the particle aggregate sizes and surface charges of CeO_2 NPs in the supernatant, the zeta potentials (ζ) and hydrodynamic particle sizes were measured (Fig. 1B and 1C). The zeta potential for stable dispersions of unreacted CeO_2 in DI water with 10 mM NaCl at pH 5.4 was 39.2 ± 3.4 mV. For the CeO_2-only system, the zeta potential was 38.6 ± 5.1 mV after 2 hr settlement. The presence of UV and 30 mM H_2O_2 decreased the absolute value of the zeta potential to 3.8 ± 3.4 mV after 2 hrs, while NOM reversed the zeta potential to -38.3 ± 1.8 mV. The lowered absolute value of the zeta potential in the presence of UV/H_2O_2 resulted in weaker electrostatic repulsive forces between CeO_2 NPs, making it easier for them to aggregate and then settle, which can explain the decreased colloidal stability of CeO_2 NPs from the UV-Vis results. However, in the presence of NOM, the absolute value of the zeta potential was close to that of unreacted CeO_2 NPs, thus maintaining the strong electrostatic repulsive forces and resisting their aggregation. When both NOM and UV/H_2O_2 were present in a system, the zeta potential was altered to -12.9 ± 2.1 mV after 2 hrs (not -38.3 ± 1.8 mV), suggesting that the effect of the NOM on the CeO_2 NPs had been changed by UV/H_2O_2.

Hydrodynamic size also provided a useful clue. The hydrodynamic particle size was 140.7 ± 53.0 nm for stable dispersions of unreacted CeO_2 in DI water at pH 5.4. After 2 hrs, for the CeO_2 NPs control system, the hydrodynamic size was 460 ± 60 nm. UV/H_2O_2 treatment increased the size to 5,574 ± 253 nm, while NOM kept the size at 175 ± 39 nm. When NOM and UV/H_2O_2 were present together, the size still increased to 3,276 ± 122 nm after 2 hr reaction. The results from the zeta potential and particle size analyses all indicated that NOM stabilized CeO_2 NPs at first, and then the reaction between NOM and UV/H_2O_2 eventually destabilized

CeO_2 NPs to form larger aggregates and settle. The zeta potential and hydrodynamic particle size values for all the conditions are also in the ESI (Table S3†).

CeO_2 NPs morphology change was monitored by HRTEM (Fig. 2). Compared with the CeO_2 control system (Fig. 2A), UV/H_2O_2 treatment resulted in forming large aggregates, helping the particles to settle (Fig. 2B). In the presence of NOM (Fig. 2C), however, CeO_2 NPs were observed to be coated with NOM, which helped to keep particles separate from each other and inhibited aggregation. Similar coatings of NOM on other nanoparticles, such as zero-valent iron, mercuric sulfide, and carbon nanotubes, have been reported before.[65-67] With UV/H_2O_2 and NOM together, after 2 hrs, the adsorbed NOM was decomposed into smaller molecules (Fig. 2D), and CeO_2 NPs were bonded closely to each other to form aggregates.

3.2 Oxidation state change of CeO_2 NPs

We hypothesized that the promoted sedimentation of suspended CeO_2 NPs exposed to UV/H_2O_2 was due to redox reactions between CeO_2 and ROS generated from UV/H_2O_2. Thus, to observe changes in the Ce oxidation states on the nanoparticle surface after 2 hrs, XPS was conducted (Fig. 3A). The Gaussian−Lorentzian curve-fitting of XPS spectra shows that CeO_2 NPs in this study had both Ce^{3+} and Ce^{4+} on the surface, while Ce^{4+} was the dominant oxidation state. Surface Ce for unreacted CeO_2 consisted of 82.2% Ce^{4+} and 17.8% Ce^{3+}. After reaction with UV/H_2O_2 for 2 hrs, surface Ce contained 71.7% Ce^{4+} and 28.3% Ce^{3+}, indicating that UV/H_2O_2 process reduced Ce^{4+} on the CeO_2 surface partially to Ce^{3+} and increased the Ce^{3+}/Ce^{4+} ratio. Based on ICP-OES data, the dissolved Ce concentration did not increase within an experimental error range in the presence of UV/H_2O_2, which indicates that the newly produced Ce^{3+} stayed on the surface of the CeO_2 NPs, rather than dissolving into solution (Table S5†). NOM itself did not change the percentage of Ce^{3+} much, but the presence of both NOM and

UV/H_2O_2 still increased the percentage of Ce^{3+} to 21.8%. As shown from XPS, in the presence of UV/H_2O_2, the redox reactions between CeO_2 and ROS resulted in an increased Ce^{3+}/Ce^{4+} ratio on the CeO_2 NPs' surfaces. This observation can partially explain the decreased surface charge of CeO_2 NPs that we observed, which can also result from other factors, such as the adsorption of negatively charged anions, discussed in section 3.4. Recent studies have shown that the redox state ratio of Ce^{3+}/Ce^{4+} on a CeO_2 surface can change the direction of the redox reaction between CeO_2 and ROS, but the fundamental mechanism behind the redox state ratio-dependent properties of CeO_2 in the presence of ROS is still elusive.[21, 22, 68-71] With a high Ce^{3+}/Ce^{4+} ratio, Ce^{3+} on the CeO_2 surface can be oxidized by $O_2^{\cdot-}$ to form Ce^{4+}, which is the SOD mimetic activity of CeO_2.[21, 69-71] On the other hand, with a low Ce^{3+}/Ce^{4+} ratio, H_2O_2 can reduce Ce^{4+} to Ce^{3+} with the oxidation of H_2O_2 to molecular O_2 and the production of protons, which is the catalase mimetic activity of CeO_2.[22, 68, 71] Similarly, here we report that Ce^{4+} can also be reduced to Ce^{3+} with a low Ce^{3+}/Ce^{4+} ratio under the UV/H_2O_2 condition, in which a pH decrease was also observed (Table S4†). This decrease reflects protons being produced from the oxidation of H_2O_2 or ·OH (eq. 5–7).[22, 68]

$$2Ce^{4+} + H_2O_2 \rightarrow 2Ce^{3+} + O_2 + 2H^+ \quad (5)$$

$$H_2O_2 \xrightarrow{UV} 2 \cdot OH \quad (6)$$

$$2Ce^{4+} + 2 \cdot OH \rightarrow 2Ce^{3+} + O_2 + 2H^+ \quad (7)$$

A systematic study of the effect of the Ce^{3+}/Ce^{4+} ratio on redox chemistry between CeO_2 NPs and ROS is an interesting future direction.

3.3 NOM adsorption on CeO_2 NPs surface

ATR-FTIR provides valuable information on the structural and functional properties of NOM molecules and their adsorption onto the CeO_2 NPs surface.[34] ATR-FTIR spectrum of unreacted CeO_2 NPs showed peaks around 585, 720, 1350, 1570, 1630, and 3400 cm^{-1}. These peaks were assigned as hydroxyl residues and bridged, bidentate, and monodentate carbonates adsorbed on the surface (Fig. S6†).[72-74] Fig. 3B shows the ATR-FTIR spectra of (**a**) NOM, (**b**) NOM adsorbed on CeO_2, and (**c**) NOM adsorbed on CeO_2 in the presence of UV/H_2O_2. The spectra **b** and **c** were obtained by subtracting the spectrum of pure CeO_2 from the spectrum of CeO_2 with NOM or NOM/UV/H_2O_2. Several peaks in the spectrum a can be identified as specific functional groups of NOM, including 1720 cm^{-1} (C–O stretching of COO^-), 1580 cm^{-1} (asymmetric stretching of COO^-), 1390 cm^{-1} (symmetrical stretching of COO^-), 1260 cm^{-1} (phenolic O–H), and 950–1125 cm^{-1} (C–O stretching) (Fig. 3B, **a**).[34, 75-77] For the NOM used, the pK_{a1} for carboxylic groups was 4.16, and the pK_{a2} for phenolic groups was 9.99,[54] thus the carboxylic portion of NOM would be partly deprotonated at pH 5.4, existing as COO^-, and the phenolic groups would mainly exist as O–H. The spectrum of the sample containing CeO_2 and NOM showed peaks at 1720, 1620, 1550, 1390, 1260, and 950–1125 cm^{-1}, confirming the adsorption of NOM on the CeO_2 surfaces (Fig. 3B, **b**). Peaks at 1720 and 1390 cm^{-1} indicated the adsorption of COO^- functional groups of NOM on the CeO_2 surface. In spectrum **b**, peak 1550 cm^{-1} could be identified as the asymmetric stretching of COO^- complexed with the CeO_2 surfaces ($CeO_2\equiv$) (eq. 8), while it shifted a bit towards lower wavenumbers compared with the carboxylate asymmetric vibrational frequencies for other metal–carboxylate complexes.[76, 78] The peak at 1620 cm^{-1} represents the adsorption of aromatic C=C or conjugated carbonyl C=O.[34, 77, 79] The peak around 1260 cm^{-1} in the spectrum **b** indicates the complexation between phenolic O–H functional groups of NOM and CeO_2 surfaces ($CeO_2\equiv$) (eq. 9).

$$CeO_2 \equiv OH_2^+ + {}^-OOC - NOM - COO^- \rightarrow CeO_2 \equiv OOC - NOM - COO^- + H_2O \quad (8)$$

$$CeO_2 \equiv OH + HO - NOM - OH \rightarrow CeO_2 \equiv O - NOM - OH + H_2O \quad (9)$$

From eq. 8, after the adsorption of NOM, the COO^- functional groups of NOM reversed the surface charge of CeO_2 NPs from positive to negative, which was observed through zeta potential measurements. When adding UV/H_2O_2 together with NOM, the peaks around 1720, 1550, 1390, 1260, and 950–1125 cm^{-1} all decreased, indicating that UV/H_2O_2 decomposed NOM adsorbed on the CeO_2 surface by breaking the COO complexation between NOM and the CeO_2 surface (Fig. 3B, c). The remaining small intensity of these peaks could be the adsorption of NOM decomposition products such as aldehydes and carboxylic acids on the CeO_2 surface,[51, 52] while the peak expansion around 1620–1660 cm^{-1} could result from the adsorption of hydroxyl-like groups produced after reaction with UV/H_2O_2.[72] XPS data for C 1s gives further evidence of NOM adsorption on CeO_2 (Fig. 3C). Three peaks were used to fit the C 1s spectra: C–C (284.8 eV), C=O (285.6 eV), and O–C=O (288.8 eV).[77] Compared with unreacted CeO_2 (Fig. 3C, a), the presence of NOM increased the total percentage of C=O and O–C=O on the CeO_2 surface from 14.0% to 36.3%, while the addition of UV/H_2O_2 into the NOM system decreased the percentages of C=O and O–C=O back to 23.0%. Detailed XPS reference binding energies for C 1s are available in the ESI (Table S6†).

To investigate the effects of NOM adsorption on the hydrophobicity/hydrophilicity of the CeO_2 NPs surface, the contact angles of a DI water drop on CeO_2-sputtered Si wafer surfaces were measured (Fig. S7A†). For an unreacted CeO_2-sputtered Si wafer, the contact angle was 82.2º ± 2.2º (Fig. S7A†, i), and after 2 hrs wetting using a 10 mM NaCl solution, the contact angle decreased to 78.2º ± 3.6º (Fig. S7A†, ii). After reaction with NOM, the contact angle decreased to 57.0º ± 2.5º (Fig. S7A†, iii). NOM has been shown to contain both hydrophobic

fractions, including humic species, and hydrophilic fractions, including carboxylic acids, carbohydrates, and amino acids.[80, 81] This decreased contact angle indicates that NOM adsorption on CeO_2 NPs makes their surfaces more hydrophilic. With the addition of UV/H_2O_2, together with NOM, the contact angle became even smaller (36.6º ± 4.2º), suggesting that the presence of both NOM and UV/H_2O_2 could make the CeO_2 surface more hydrophilic (Fig. S7†, iv). Regardless of this increased hydrophilicity, however, CeO_2 NPs tended to aggregate more. This observation indicates that factors other than hydrophilicity, such as steric interactions and electrostatic repulsive forces, are dominant in affecting CeO_2 colloidal stability.

3.4 Dominant reaction mechanisms

To provide a more detailed mechanism explaining the decreased colloidal stability of CeO_2 NPs during treatment with UV/H_2O_2, ROS scavenging experiments were conducted using UV-Vis and XPS to elucidate the role of two radicals, $O_2^{\cdot-}$ and ·OH, in changing the surface chemistry of CeO_2 NPs (Fig. 4). Fig. 4A shows the UV-Vis absorbance of CeO_2 at elapsed times under different reaction conditions. Here, SOD was utilized to quench $O_2^{\cdot-}$ ($k = 1.79 \times 10^9$ M^{-1} s^{-1})[15], and t-ButOH was used to quench ·OH ($k = 6 \times 10^8$ M^{-1} s^{-1})[63]. In the presence of SOD, the sedimentation of CeO_2 NPs slowed significantly, indicating that $O_2^{\cdot-}$ played an important role in destabilizing CeO_2. After the addition of t-ButOH, the sedimentation of CeO_2 NPs was further promoted compared to the system with only UV/H_2O_2. This finding suggests that ·OH and $O_2^{\cdot-}$ affect the colloidal stability of CeO_2 differently: $O_2^{\cdot-}$ promotes the sedimentation of CeO_2, while ·OH inhibits the sedimentation of CeO_2.

To better understand the surface oxygen species on CeO_2 surfaces after the reaction, the O 1s spectra from XPS were fitted with four peak contributions, referred to as O_I, O_{II}, O_{III}, and O_{IV} peaks (Fig. 4B). The major peak O_I (BE ≈ 528.6–529.0 eV) is characteristic of lattice oxygen

in CeO_2.[82, 83] Peak O_{III} (BE ≈ 531.3–532.0 eV) belongs most likely to hydroxyl-like groups,[84-86] and peak O_{IV} (BE ≈ 533.5–534.3 eV) is characteristic of residual adsorbed H_2O.[87] In the presence of UV/H_2O_2 (Fig. 4B, b), the area ratio of peak O_{II} (BE ≈ 530.1–530.7 eV) was 36.8%, much higher than that of unreacted CeO_2 (11.5%, Table S5). The presence of t-ButOH further increased the ratio of peak O_{II} to 48.0% (Fig. 4B, c). In contrast, the presence of SOD decreased the ratio of peak O_{II} back to 18.2% (Fig. 4B, d). These results indicate that the increase of peak O_{II} may involve the bonding of $O_2^{\cdot-}$ with the CeO_2 surface. In earlier reports, peak O_{II} (530–531 eV) has been assigned to provide evidence for chemisorbed molecular oxygen species such as peroxo-like species[87-89] or superoxo-like species[90], although most of them are dealing with other nanoparticles than CeO_2. Peak O_{II} has also been reported to result from carbonates.[91] However, with the pH conditions in this study, the dissolved CO_2 in the solution for different systems would be similar, thus the contribution of carbonates to the peak O_{II} should be similar.[87] Based on UV-Vis results, $O_2^{\cdot-}$ played the main role in promoting the sedimentation of CeO_2, and its negative charge was capable of neutralizing the positive surface charge of CeO_2. Thus, we deduce that the bonding of $O_2^{\cdot-}$ with the CeO_2 surface contributes dominantly to the increase of peak O_{II}. The ability of $O_2^{\cdot-}$ to bond with the CeO_2 surface has also been reported by other studies.[92] It should be noted that XPS results could not directly show the adsorption of $O_2^{\cdot-}$ radicals onto CeO_2 surface, because $O_2^{\cdot-}$ would change into oxygen bonding after the adsorption. However, this consequent oxygen bonding shown by XPS still suggests the adsorption of metastable molecular oxygen species onto the CeO_2 surface during the reaction.

Summarizing the results of the UV-Vis and XPS experiments, a mechanism regarding the reaction between CeO_2 NPs and ROS was proposed, shown in Fig. 5. Before reaction with ROS, CeO_2 NPs contained relatively a lower ratio of Ce^{3+}/Ce^{4+} (stage I). During UV/H_2O_2 process, the

ROS generated, such as ·OH and $O_2^{\cdot-}$, reacted with CeO_2, reducing part of the Ce^{4+} to Ce^{3+} on the CeO_2 surface and increasing the ratio of Ce^{3+}/Ce^{4+}. During this process, protons were released, which contributed to the decreased pH values observed. Oxygen molecules were also generated from the oxidation of H_2O_2 or ·OH by CeO_2.[22, 68] At stage I, the CeO_2 surface was positively charged due to surface adsorbed hydroxyl functional groups such as $–OH_2^+$.[34, 93, 94] From stage I to stage II, $O_2^{\cdot-}$ radicals adsorbed onto the CeO_2 surface by exchanging with $–OH_2^+$ functional groups and neutralized the surface charge of CeO_2, as observed from zeta potential measurements. A lowered surface charge resulted in smaller electrostatic repulsive forces between nanoparticles, making them aggregate and settle. The electron from each adsorbed $O_2^{\cdot-}$ could be transferred to or shared with one Ce^{4+} ion on the CeO_2 surface, making it form Ce^{3+}. This formation might be the reason for the observed higher ratio of Ce^{3+} on the CeO_2 surface in our systems, but we still will need a separate future study to confirm this interesting point.

4. Conclusions and Environmental Implications

The wide applications of engineered nanomaterials in industry have increased their chances of entering into engineered water treatment processes, including AOPs. Our work, for the first time, systematically evaluated the co-effects of NOM and ROS on the surface properties, colloidal stability, and aggregation of CeO_2 NPs in simulated AOPs. It was found that UV/H_2O_2 promoted CeO_2 NPs sedimentation by neutralizing the surface charge of NPs, while NOM helped to stabilize CeO_2 NPs by reversing the surface charge of NPs and maintaining the electrostatic repulsive forces. In the presence of NOM and UV/H_2O_2 together, however, NOM on CeO_2 NPs acted as a protective layer, which made the reactions between CeO_2 NPs and ROS insignificant in a shorter reaction period. The roles of different types of ROS in changing the surface chemistry and colloidal stability of CeO_2 NPs were also evaluated. In the experimental

system, the adsorption of superoxide radicals ($O_2^{\cdot-}$) dominated in neutralizing the surface charge of CeO_2 NPs compared with other ROS, such as hydroxyl radicals (·OH). Previously the redox reactions between ROS and CeO_2 NPs (in particular, the change of the Ce^{3+}/ Ce^{4+} ratio on the surface) were mainly considered, but in this study, we showed that ROS could have surface complexation with CeO_2 NPs and change their surface charge, which leads to the aggregation and sedimentation of NPs.

The results have significant implications for better understanding the fate and transport of CeO_2 NPs in WWTPs (in particular, AOPs). Organic matter, such as NOM, can help to stabilize CeO_2 NPs through surface complexation and by changing the steric interactions between NPs. Therefore, it is likely that CeO_2 NPs associated with NOM will be transported in wastewater without much sedimentation and removal, increasing their transport distances and potentially increasing their concentration in the secondary effluents. The complexation mechanism of NOM on CeO_2 NPs, its effect on CeO_2 NPs' surface charge and hydrophilicity, and the alleviation of the CeO_2 NPs-ROS reaction by NOM coating can all contribute to a mechanistic understanding of the effects of organic matter on the fate and transport of CeO_2 NPs in WWTPs.

CeO_2 NPs in WWTPs can also form complexes with other types of organic matter, including SMPs which contain higher fractions of hydrophilic constituents (i.e., polysaccharides and proteins) than NOM.[28-31] Considering that NOM is an organic macromolecule that contains many of the same functional groups that occur in cellular debris, it is a useful probe molecule to provide insights into the role of organic matter in changing the fundamental chemistry of CeO_2 NPs in the UV/H_2O_2 system. However, the effects of different types of organic matter in WWTPs (i.e., NOM, SMPs, and EfOM) on the aggregation of CeO_2 NPs in AOPs should all be carefully studied and compared in the future. After the CeO_2 NPs and organic matter complexes

enter AOPs, the ROS can decompose the organic matter coated on CeO_2 NPs surface and also reduce the colloidal stability of CeO_2 NPs through the neutralization of their surface charge, which can lead to the sedimentation of NPs. Thus, AOPs could possibly provide another mechanism to remove and recover CeO_2 NPs from secondary effluents. In the future, besides different organic matter types, more efforts should also be devoted to evaluate the effects of water chemistry (i.e., pH values, ionic strength) and water constituents (i.e., cations, anions) on the fate of CeO_2 NPs or other engineered nanomaterials in AOPs.

Our findings also have intriguing implications for other research areas. For example, in natural water systems, it is also possible for CeO_2 NPs to meet NOM and ROS together. Our results will help to predict CeO_2 NPs' fate under such circumstances. Furthermore, because of the free-radical-scavenging property of CeO_2 NPs, there have been many studies discussing using them as antioxidants for cells to resist the ROS-induced cell injury.[95-97] Our study also suggests that in such biomedical applications, CeO_2 NPs might aggregate after their reaction with ROS, especially $O_2^{\cdot-}$. The toxicity of aggregated CeO_2 NPs to normal cells, the influence of CeO_2 NPs aggregation on their therapeutic behavior, and their transport in the body should be carefully elucidated.

Conflicts of interest

There are no conflicts to declare.

Acknowledgements

We are grateful for support received from the Environmental Chemical Science program of the National Science Foundation (CHE-1214090). We wish to thank the Institute of Materials

Science and Engineering (IMSE) in Washington University in St. Louis for the use of a clean room, XPS, and HRTEM. We also thank the Nano Research Facility (NRF) at Washington University in St. Louis for use of ICP-OES and ultracentrifuge. Thank Prof. James Ballard for carefully reviewing our manuscript. Lastly, we also thank the Environmental NanoChemistry Group members for providing valuable discussions and suggestions for this paper.

Literature Cited

1. K. Reed, A. Cormack, A. Kulkarni, M. Mayton, D. Sayle, F. Klaessig and B. Stadler, Exploring the properties and applications of nanoceria: is there still plenty of room at the bottom? *Environ. Sci. Nano.*, 2014, **1**, 390-405.
2. A. A. Keller, S. McFerran, A. Lazareva and S. Suh, Global life cycle releases of engineered nanomaterials, *J. Nanopart. Res.*, 2013, **15**, 1-17.
3. L. E. Barton, M. Auffan, M. Bertrand, M. Barakat, C. Santaella, A. Masion, D. Borschneck, L. Olivi, N. Roche and M. R. Wiesner, Transformation of pristine and citrate-functionalized CeO_2 nanoparticles in a laboratory-scale activated sludge reactor, *Environ. Sci. Technol.*, 2014, **48**, 7289-7296.
4. L. E. Barton, M. Auffan, L. Olivi, J.-Y. Bottero and M. R. Wiesner, Heteroaggregation, transformation and fate of CeO_2 nanoparticles in wastewater treatment, *Environ. Pollut.*, 2015, **203**, 122-129.
5. B. Collin, M. Auffan, A. C. Johnson, I. Kaur, A. A. Keller, A. Lazareva, J. R. Lead, X. Ma, R. C. Merrifield and C. Svendsen, Environmental release, fate and ecotoxicological effects of manufactured ceria nanomaterials, *Environ. Sci. Nano.*, 2014, **1**, 533-548.
6. F. Gómez-Rivera, J. A. Field, D. Brown and R. Sierra-Alvarez, Fate of cerium dioxide (CeO_2) nanoparticles in municipal wastewater during activated sludge treatment, *Bioresour. Technol.*, 2012, **108**, 300-304.
7. L. K. Limbach, R. Bereiter, E. Müller, R. Krebs, R. Gälli and W. J. Stark, Removal of oxide nanoparticles in a model wastewater treatment plant: influence of agglomeration and surfactants on clearing efficiency, *Environ. Sci. Technol.*, 2008, **42**, 5828-5833.
8. V. H. Grassian, A. J. Haes, I. A. Mudunkotuwa, P. Demokritou, A. B. Kane, C. J. Murphy, J. E. Hutchison, J. A. Isaacs, Y.-S. Jun and B. Karn, NanoEHS–defining fundamental science needs: no easy feat when the simple itself is complex, *Environ. Sci. Nano.*, 2016, **3**, 15-27.
9. W. Lin, Y.-w. Huang, X.-D. Zhou and Y. Ma, Toxicity of cerium oxide nanoparticles in human lung cancer cells, *Int. J. Toxicol.*, 2006, **25**, 451-457.
10. E.-J. Park, J. Choi, Y.-K. Park and K. Park, Oxidative stress induced by cerium oxide nanoparticles in cultured BEAS-2B cells, *Toxicology*, 2008, **245**, 90-100.
11. R. Andreozzi, V. Caprio, A. Insola and R. Marotta, Advanced oxidation processes (AOP) for water purification and recovery, *Catal. Today*, 1999, **53**, 51-59.
12. S. Parsons, *Advanced oxidation processes for water and wastewater treatment*, IWA publishing, 2004.
13. M. Pera-Titus, V. Garcıa-Molina, M. A. Baños, J. Giménez and S. Esplugas, Degradation of chlorophenols by means of advanced oxidation processes: a general review, *Appl. Catal., B*, 2004, **47**, 219-256.
14. A. Stasinakis, Use of selected advanced oxidation processes (AOPs) for wastewater treatment—a mini review, *Global NEST J.*, 2008, **10**, 376-385.
15. B. H. Bielski, D. E. Cabelli, R. L. Arudi and A. B. Ross, Reactivity of HO_2/O^{-2} radicals in aqueous solution, *J. Phys. Chem. Ref. Data*, 1985, **14**, 1041-1100.
16. G. V. Buxton, C. L. Greenstock, W. P. Helman and A. B. Ross, Critical review of rate constants for reactions of hydrated electrons, hydrogen atoms and hydroxyl radicals ($\cdot OH/\cdot O^-$) in aqueous solution, *J. Phys. Chem. Ref. Data*, 1988, **17**, 513-886.

17. H. Christensen, K. Sehested and H. Corfitzen, Reactions of hydroxyl radicals with hydrogen peroxide at ambient and elevated temperatures, *J. Phys. Chem.*, 1982, **86**, 1588-1590.
18. S. M. Hirst, A. S. Karakoti, R. D. Tyler, N. Sriranganathan, S. Seal and C. M. Reilly, Anti-inflammatory Properties of Cerium Oxide Nanoparticles, *Small*, 2009, 5, 2848-2856.
19. I. Celardo, M. De Nicola, C. Mandoli, J. Z. Pedersen, E. Traversa and L. Ghibelli, Ce^{3+} ions determine redox-dependent anti-apoptotic effect of cerium oxide nanoparticles, *ACS Nano*, 2011, 5, 4537-4549.
20. M. Das, S. Patil, N. Bhargava, J.-F. Kang, L. M. Riedel, S. Seal and J. J. Hickman, Auto-catalytic ceria nanoparticles offer neuroprotection to adult rat spinal cord neurons, *Biomaterials*, 2007, **28**, 1918-1925.
21. E. G. Heckert, A. S. Karakoti, S. Seal and W. T. Self, The role of cerium redox state in the SOD mimetic activity of nanoceria, *Biomaterials*, 2008, **29**, 2705-2709.
22. T. Pirmohamed, J. M. Dowding, S. Singh, B. Wasserman, E. Heckert, A. S. Karakoti, J. E. King, S. Seal and W. T. Self, Nanoceria exhibit redox state-dependent catalase mimetic activity, *Chem. Commun.*, 2010, **46**, 2736-2738.
23. C. Jarusutthirak, G. Amy and J.-P. Croué, Fouling characteristics of wastewater effluent organic matter (EfOM) isolates on NF and UF membranes, *Desalination*, 2002, **145**, 247-255.
24. C. N. Laabs, G. L. Amy and M. Jekel, Understanding the size and character of fouling-causing substances from effluent organic matter (EfOM) in low-pressure membrane filtration, *Environ. Sci. Technol.*, 2006, **40**, 4495-4499.
25. H. Shon, S. Vigneswaran and S. Snyder, Effluent Organic Matter (EfOM) in Wastewater: Constituents, Effects, and Treatment, *Crit. Rev. Environ. Sci. Technol.*, 2006, **36**, 327-374.
26. M. M. Bazri, B. Barbeau and M. Mohseni, Impact of UV/H_2O_2 advanced oxidation treatment on molecular weight distribution of NOM and biostability of water, *Water Res.*, 2012, **46**, 5297-5304.
27. A. Chin and P. Bérubé, Removal of disinfection by-product precursors with ozone-UV advanced oxidation process, *Water Res.*, 2005, **39**, 2136-2144.
28. J. E. Drewes and P. Fox, Fate of natural organic matter (NOM) during groundwater recharge using reclaimed water, *Water Sci. Technol.*, 1999, **40**, 241-248.
29. C. Jarusutthirak and G. Amy, Role of soluble microbial products (SMP) in membrane fouling and flux decline, *Environ. Sci. Technol.*, 2006, **40**, 969-974.
30. J.-l. Liu, X.-y. Li, Y.-f. Xie and H. Tang, Characterization of soluble microbial products as precursors of disinfection byproducts in drinking water supply, *Sci. Total Environ.*, 2014, **472**, 818-824.
31. Y.-x. Shen, K. Xiao, P. Liang, J.-y. Sun, S.-j. Sai and X. Huang, Characterization of soluble microbial products in 10 large-scale membrane bioreactors for municipal wastewater treatment in China, *J. Membr. Sci. Technol.*, 2012, **415**, 336-345.
32. B. Koch and T. Dittmar, From mass to structure: an aromaticity index for high resolution mass data of natural organic matter, *Rapid Commun. Mass Spectrom.*, 2006, **20**, 926-932.
33. G. R. Aiken, H. Hsu-Kim and J. N. Ryan, Influence of dissolved organic matter on the environmental fate of metals, nanoparticles, and colloids, *Environ. Sci. Technol.*, 2011, **45**, 3196-3201.

34. B. Gu, J. Schmitt, Z. Chen, L. Liang and J. F. McCarthy, Adsorption and desorption of natural organic matter on iron oxide: mechanisms and models, *Environ. Sci. Technol.*, 1994, **28**, 38-46.
35. G. Sposito, *The surface chemistry of soils*, 1984.
36. C. L. Tiller and C. R. O'Melia, Natural organic matter and colloidal stability: models and measurements, *Colloids Surf., A*, 1993, **73**, 89-102.
37. M. Delay, T. Dolt, A. Woellhaf, R. Sembritzki and F. H. Frimmel, Interactions and stability of silver nanoparticles in the aqueous phase: Influence of natural organic matter (NOM) and ionic strength, *J. Chromatogr., A*, 2011, **1218**, 4206-4212.
38. O. Furman, S. Usenko and B. L. Lau, Relative importance of the humic and fulvic fractions of natural organic matter in the aggregation and deposition of silver nanoparticles, *Environ. Sci. Technol.*, 2013, **47**, 1349-1356.
39. H. Hyung, J. D. Fortner, J. B. Hughes and J.-H. Kim, Natural organic matter stabilizes carbon nanotubes in the aqueous phase, *Environ. Sci. Technol.*, 2007, **41**, 179-184.
40. S. M. Louie, R. D. Tilton and G. V. Lowry, Effects of molecular weight distribution and chemical properties of natural organic matter on gold nanoparticle aggregation, *Environ. Sci. Technol.*, 2013, **47**, 4245-4254.
41. D. P. Stankus, S. E. Lohse, J. E. Hutchison and J. A. Nason, Interactions between natural organic matter and gold nanoparticles stabilized with different organic capping agents, *Environ. Sci. Technol.*, 2010, **45**, 3238-3244.
42. E. M. Murphy, J. M. Zachara, S. C. Smith and J. L. Phillips, The sorption of humic acids to mineral surfaces and their role in contaminant binding, *Sci. Total Environ.*, 1992, **117**, 413-423.
43. A. A. Keller, H. Wang, D. Zhou, H. S. Lenihan, G. Cherr, B. J. Cardinale, R. Miller and Z. Ji, Stability and aggregation of metal oxide nanoparticles in natural aqueous matrices, *Environ. Sci. Technol.*, 2010, **44**, 1962-1967.
44. J. T. Quik, I. Lynch, K. Van Hoecke, C. J. Miermans, K. A. De Schamphelaere, C. R. Janssen, K. A. Dawson, M. A. C. Stuart and D. Van De Meent, Effect of natural organic matter on cerium dioxide nanoparticles settling in model fresh water, *Chemosphere*, 2010, **81**, 711-715.
45. Z. Zhang, P. Gao, Y. Qiu, G. Liu, Y. Feng and M. Wiesner, Transport of cerium oxide nanoparticles in saturated silica media: influences of operational parameters and aqueous chemical conditions, *Scientific reports*, 2016, **6**.
46. B. Collin, E. Oostveen, O. V. Tsyusko and J. M. Unrine, Influence of natural organic matter and surface charge on the toxicity and bioaccumulation of functionalized ceria nanoparticles in Caenorhabditis elegans, *Environ. Sci. Technol.*, 2014, **48**, 1280-1289.
47. A. Kroll, R. Behra, R. Kaegi and L. Sigg, Extracellular polymeric substances (EPS) of freshwater biofilms stabilize and modify CeO_2 and Ag nanoparticles, *PLoS One*, 2014, **9**, e110709.
48. T. Kikuchi, M. Fujii, K. Terao, R. Jiwei, Y. P. Lee and C. Yoshimura, Correlations between aromaticity of dissolved organic matter and trace metal concentrations in natural and effluent waters: A case study in the Sagami River Basin, Japan, *Sci. Total Environ.*, 2017, **576**, 36-45.
49. L. Yang, H.-S. Shin and J. Hur, Estimating the concentration and biodegradability of organic matter in 22 wastewater treatment plants using fluorescence excitation emission matrices and parallel factor analysis, *Sensors*, 2014, **14**, 1771-1786.

50. P. Westerhoff, S. P. Mezyk, W. J. Cooper and D. Minakata, Electron pulse radiolysis determination of hydroxyl radical rate constants with Suwannee River fulvic acid and other dissolved organic matter isolates, *Environ. Sci. Technol.*, 2007, **41**, 4640-4646.
51. J. Thomson, F. A. Roddick and M. Drikas, Vacuum ultraviolet irradiation for natural organic matter removal, *J. Water Supply Res. T.*, 2004, **53**, 193-206.
52. S. R. Sarathy and M. Mohseni, The impact of UV/H_2O_2 advanced oxidation on molecular size distribution of chromophoric natural organic matter, *Environ. Sci. Technol.*, 2007, **41**, 8315-8320.
53. S. Sarathy and M. Mohseni, The fate of natural organic matter during UV/H_2O_2 advanced oxidation of drinking water A paper submitted to the Journal of Environmental Engineering and Science, *Can. J. Civ. Eng.*, 2008, **36**, 160-169.
54. C. W. Neil, J. R. Ray, B. Lee and Y.-S. Jun, Fractal aggregation and disaggregation of newly formed iron (iii)(hydr) oxide nanoparticles in the presence of natural organic matter and arsenic, *Environ. Sci. Nano.*, 2016, **3**, 647-656.
55. M.-W. Chang, C.-C. Chung, J.-M. Chern and T.-S. Chen, Dye decomposition kinetics by UV/H_2O_2: initial rate analysis by effective kinetic modelling methodology, *Chem. Eng. Sci.*, 2010, **65**, 135-140.
56. X. Liu, J. R. Ray, C. W. Neil, Q. Li and Y.-S. Jun, Enhanced Colloidal Stability of CeO_2 Nanoparticles by Ferrous Ions: Adsorption, Redox Reaction, and Surface Precipitation, *Environ. Sci. Technol.*, 2015, **49**, 5476-5483.
57. N. Daneshvar, M. Behnajady, M. K. A. Mohammadi and M. S. Dorraji, UV/H_2O_2 treatment of Rhodamine B in aqueous solution: Influence of operational parameters and kinetic modeling, *Desalination*, 2008, **230**, 16-26.
58. M. Muruganandham and M. Swaminathan, Photochemical oxidation of reactive azo dye with UV–H_2O_2 process, *Dyes Pigm.*, 2004, **62**, 269-275.
59. P. W. Park and J. S. Ledford, Effect of crystallinity on the photoreduction of cerium oxide: A study of CeO_2 and Ce/Al_2O_3 catalysts, *Langmuir*, 1996, **12**, 1794-1799.
60. K.-D. Schierbaum, Ordered ultra-thin cerium oxide overlayers on Pt (111) single crystal surfaces studied by LEED and XPS, *Surf. Sci.*, 1998, **399**, 29-38.
61. S. Deshpande, S. Patil, S. V. Kuchibhatla and S. Seal, Size dependency variation in lattice parameter and valency states in nanocrystalline cerium oxide, *Appl. Phys. Lett.*, 2005, **87**, 133113-133113.
62. F. Zhang, P. Wang, J. Koberstein, S. Khalid and S.-W. Chan, Cerium oxidation state in ceria nanoparticles studied with X-ray photoelectron spectroscopy and absorption near edge spectroscopy, *Surf. Sci.*, 2004, **563**, 74-82.
63. A. Aguila, K. E. O'Shea, T. Tobien and K.-D. Asmus, Reactions of hydroxyl radical with dimethyl methylphosphonate and diethyl methylphosphonate. A fundamental mechanistic study, *J. Phys. Chem. A.*, 2001, **105**, 7834-7839.
64. J. M. McCord and I. Fridovich, Superoxide dismutase an enzymic function for erythrocuprein (hemocuprein), *J. Biol. Chem.*, 1969, **244**, 6049-6055.
65. J. Chen, Z. Xiu, G. V. Lowry and P. J. Alvarez, Effect of natural organic matter on toxicity and reactivity of nano-scale zero-valent iron, *Water Res.*, 2011, **45**, 1995-2001.
66. A. Deonarine and H. Hsu-Kim, Precipitation of mercuric sulfide nanoparticles in NOM-containing water: Implications for the natural environment, *Environ. Sci. Technol.*, 2009, **43**, 2368-2373.

67. H. Hyung and J.-H. Kim, Natural organic matter (NOM) adsorption to multi-walled carbon nanotubes: effect of NOM characteristics and water quality parameters, *Environ. Sci. Technol.*, 2008, **42**, 4416-4421.
68. I. Celardo, J. Z. Pedersen, E. Traversa and L. Ghibelli, Pharmacological potential of cerium oxide nanoparticles, *Nanoscale*, 2011, **3**, 1411-1420.
69. A. S. Karakoti, S. Singh, A. Kumar, M. Malinska, S. V. Kuchibhatla, K. Wozniak, W. T. Self and S. Seal, PEGylated nanoceria as radical scavenger with tunable redox chemistry, *J. Am. Chem. Soc.*, 2009, **131**, 14144-14145.
70. C. Korsvik, S. Patil, S. Seal and W. T. Self, Superoxide dismutase mimetic properties exhibited by vacancy engineered ceria nanoparticles, *Chem. Commun.*, 2007, 1056-1058.
71. S. Singh, T. Dosani, A. S. Karakoti, A. Kumar, S. Seal and W. T. Self, A phosphate-dependent shift in redox state of cerium oxide nanoparticles and its effects on catalytic properties, *Biomaterials*, 2011, **32**, 6745-6753.
72. E. Kumar, P. Selvarajan and K. Balasubramanian, Preparation and studies of cerium dioxide (CeO_2) nanoparticles by microwave-assisted solution method, *Recent Res. Sci. Technol.*, 2010, **2**.
73. C. Li, Y. Sakata, T. Arai, K. Domen, K.-i. Maruya and T. Onishi, Adsorption of carbon monoxide and carbon dioxide on cerium oxide studied by Fourier-transform infrared spectroscopy. Part 2.-Formation of formate species on partially reduced CeO_2 at room temperature, *J. Chem. Soc., Faraday Trans. 1*, 1989, **85**, 1451-1461.
74. C. Li, Y. Sakata, T. Arai, K. Domen, K.-i. Maruya and T. Onishi, Carbon monoxide and carbon dioxide adsorption on cerium oxide studied by Fourier-transform infrared spectroscopy. Part 1.-Formation of carbonate species on dehydroxylated CeO_2, at room temperature, *J. Chem. Soc., Faraday Trans. 1*, 1989, **85**, 929-943.
75. J. Cho, G. Amy, J. Pellegrino and Y. Yoon, Characterization of clean and natural organic matter (NOM) fouled NF and UF membranes, and foulants characterization, *Desalination*, 1998, **118**, 101-108.
76. S. K. Papageorgiou, E. P. Kouvelos, E. P. Favvas, A. A. Sapalidis, G. E. Romanos and F. K. Katsaros, Metal–carboxylate interactions in metal–alginate complexes studied with FTIR spectroscopy, *Carbohydr. Res.*, 2010, **345**, 469-473.
77. W.-L. Sun, J. Xia, S. Li and F. Sun, Effect of natural organic matter (NOM) on Cu (II) adsorption by multi-walled carbon nanotubes: relationship with NOM properties, *Chem. Eng. J.*, 2012, **200**, 627-636.
78. X.-H. Guan, C. Shang and G.-H. Chen, ATR-FTIR investigation of the role of phenolic groups in the interaction of some NOM model compounds with aluminum hydroxide, *Chemosphere*, 2006, **65**, 2074-2081.
79. J. Chen, B. Gu, E. J. LeBoeuf, H. Pan and S. Dai, Spectroscopic characterization of the structural and functional properties of natural organic matter fractions, *Chemosphere*, 2002, **48**, 59-68.
80. T. Bond, E. H. Goslan, S. A. Parsons and B. Jefferson, A critical review of trihalomethane and haloacetic acid formation from natural organic matter surrogates, *Environ. Technol. Rev.*, 2012, **1**, 93-113.
81. J.-P. Croue, G. V. Korshin and M. M. Benjamin, *Characterization of natural organic matter in drinking water*, American Water Works Association, 2000.

82. A. Bensalem, F. Bozon-Verduraz, M. Delamar and G. Bugli, Preparation and characterization of highly dispersed silica-supported ceria, *Appl. Catal., A*, 1995, **121**, 81-93.
83. S. Hamoudi, F. ç. Larachi, A. Adnot and A. Sayari, Characterization of spent MnO_2/CeO_2 wet oxidation catalyst by TPO–MS, XPS, and S-SIMS, *J. Catal.*, 1999, **185**, 333-344.
84. H. Chen, A. Sayari, A. Adnot and F. ç. Larachi, Composition–activity effects of Mn–Ce–O composites on phenol catalytic wet oxidation, *Appl. Catal., B*, 2001, **32**, 195-204.
85. A. Laachir, V. Perrichon, A. Badri, J. Lamotte, E. Catherine, J. C. Lavalley, J. El Fallah, L. Hilaire, F. Le Normand and E. Quéméré, Reduction of CeO_2 by hydrogen. Magnetic susceptibility and Fourier-transform infrared, ultraviolet and X-ray photoelectron spectroscopy measurements, *J. Chem. Soc., Faraday Trans.*, 1991, **87**, 1601-1609.
86. F. ç. Larachi, J. Pierre, A. Adnot and A. Bernis, Ce 3d XPS study of composite $Ce_xMn_{1-x}O_{2-y}$ wet oxidation catalysts, *Appl. Surf. Sci.*, 2002, **195**, 236-250.
87. F. Scholes, A. Hughes, S. Hardin, P. Lynch and P. Miller, Influence of hydrogen peroxide in the preparation of nanocrystalline ceria, *Chem. Mater.*, 2007, **19**, 2321-2328.
88. Y. Dai, A. Manthiram, A. Campion and J. Goodenough, X-ray-photoelectron-spectroscopy evidence for peroxide in 1: 2: 3 copper oxides containing disordered or excess oxygen, *Phys. Rev. B*, 1988, **38**, 5091.
89. B. Lamontagne, D. Roy, R. Sporken and R. Caudano, Identification of the adsorption sites of molecular oxygen on Si (111) using XPS, *Prog. Surf. Sci.*, 1995, **50**, 315-324.
90. C. T. Campbell, An XPS study of molecularly chemisorbed oxygen on Ag (111), *Surf. Sci.*, 1986, **173**, L641-L646.
91. A. Hughes, R. Taylor, B. Hinton and L. Wilson, XPS and SEM characterization of hydrated cerium oxide conversion coatings, *Surf. Interface Anal.*, 1995, **23**, 540-550.
92. J. Soria, A. Martinez-Arias and J. Conesa, Effect of oxidized rhodium on oxygen adsorption on cerium oxide, *Vacuum*, 1992, **43**, 437-440.
93. H. Boehm, Acidic and basic properties of hydroxylated metal oxide surfaces, *Disc. Faraday Soc.*, 1971, **52**, 264-275.
94. S. Goldberg, Competitive adsorption of arsenate and arsenite on oxides and clay minerals, *Soil Sci. Soc. Am. J.*, 2002, **66**, 413-421.
95. A. Asati, S. Santra, C. Kaittanis and J. M. Perez, Surface-charge-dependent cell localization and cytotoxicity of cerium oxide nanoparticles, *ACS nano*, 2010, **4**, 5321-5331.
96. A. Karakoti, N. Monteiro-Riviere, R. Aggarwal, J. Davis, R. J. Narayan, W. Self, J. McGinnis and S. Seal, Nanoceria as antioxidant: synthesis and biomedical applications, *Jom*, 2008, **60**, 33-37.
97. R. W. Tarnuzzer, J. Colon, S. Patil and S. Seal, Vacancy engineered ceria nanostructures for protection from radiation-induced cellular damage, *Nano Lett.*, 2005, **5**, 2573-2577.

List of Figures

Fig. 1 (A) UV-Vis data showing the sedimentation of CeO_2 NPs at 10 mM NaCl and pH 5.4 in the presence and absence of UV/H_2O_2 (30 mM) and NOM (3.3 ± 0.2 mg C/L). The percentages were obtained by normalizing the suspended nanoparticle concentration by the initial concentration. (B) Zeta potential results for CeO_2 NPs in the presence and absence of UV/H_2O_2 (30 mM) and NOM. The zeta potential for stable dispersions of unreacted CeO_2 in DI water with 10 mM NaCl at pH 5.4 was 39.2 ± 3.4 mV. (C) Hydrodynamic particle size values for CeO_2 NPs in the presence and absence of UV/H_2O_2 (30 mM) and NOM. The error bars represent the standard deviation from triplicate experiments. Only representative conditions are presented here, and other detailed results are provided in the ESI (Fig. S4† and Table S2†).

Fig. 2 Representative TEM images for CeO_2 NPs with 10 mM NaCl at pH 5.4 after 2 hrs. (A) CeO_2 control, (B) CeO_2 with UV/H_2O_2, (C) CeO_2 with NOM, and (D) CeO_2 with NOM and UV/H_2O_2.

Fig. 3 (A) XPS spectra of Ce 3d obtained from CeO_2 sedimentation with 10 mM NaCl at pH 5.4 after 2 hrs reaction. (a) CeO_2 control, (b) CeO_2 with UV/H_2O_2, (c) CeO_2 with NOM, and (d) CeO_2 with NOM and UV/H_2O_2. Dotted lines show the position of two different Ce^{3+} peaks: Ce^{3+} $3d_{5/2}$ and Ce^{3+} $3d_{3/2}$. The red curves are the Gaussian−Lorentzian curve-fitting of XPS spectra. The variation of calculated Ce^{3+} and Ce^{4+} percentages from the fitting of at least triplicate samples was within ±1%. (B) FTIR spectra of CeO_2 sedimentation with 10 mM NaCl at pH 5.4 after 2 hrs reaction. (a) NOM, (b) NOM reacted with CeO_2, (c) NOM reacted with CeO_2 and UV/H_2O_2. The spectra of NOM with CeO_2 and NOM with CeO_2/UV/H_2O_2 (b and c)

were obtained by subtracting the spectrum of pure CeO_2 from their measured spectra. (C) XPS spectra of C 1s obtained from CeO_2 sedimentation with 10 mM NaCl at pH 5.4 after 2 hrs reaction. (a) CeO_2 control, (b) CeO_2 with UV/H_2O_2, (c) CeO_2 with NOM, and (d) CeO_2 with NOM and UV/H_2O_2.

Fig. 4 (A) CeO_2 NP concentration measured by UV-Vis with 10 mM NaCl at pH 5.4 with SOD and t-ButOH. Dotted lines are control experiments with only SOD and t-ButOH. The percentages were obtained from the suspended nanoparticle concentrations normalized by the initial suspended concentration. The error bars represent the standard deviation of CeO_2 NP concentrations from triplicate experiments. (B) XPS spectra of O 1s obtained from CeO_2 sedimentation with 10 mM NaCl at pH 5.4 after 2 hrs reaction. (a) CeO_2 control, (b) CeO_2 with UV/H_2O_2, (c) CeO_2 with UV/H_2O_2 and t-ButOH, and (d) CeO_2 with with UV/H_2O_2 and SOD.

Fig. 5 Schematic diagram for the proposed mechanism of the reaction between CeO_2 and ROS generated during UV/H_2O_2 exposure.

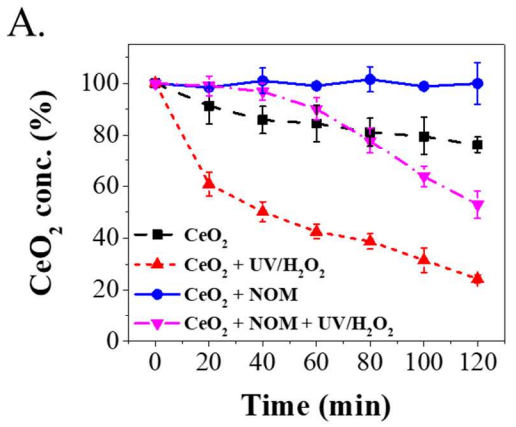
A.
CeO_2 conc. (%)
100
80
60
40
20
0
0 20 40 60 80 100 120
Time (min)
CeO_2
CeO_2 + UV/H_2O_2
CeO_2 + NOM
CeO_2 + NOM + UV/H_2O_2

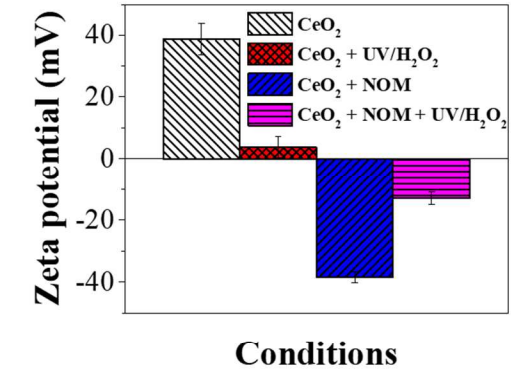
B.
Zeta potential (mV)
40
20
0
-20
-40
Conditions
CeO_2
CeO_2 + UV/H_2O_2
CeO_2 + NOM
CeO_2 + NOM + UV/H_2O_2

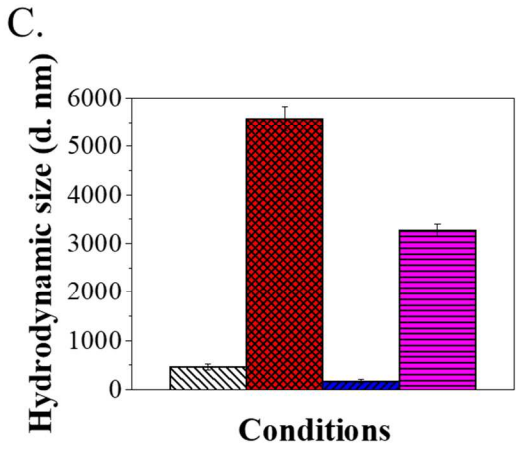
C.
Hydrodynamic size (d. nm)
6000
5000
4000
3000
2000
1000
0
Conditions

Fig. 1

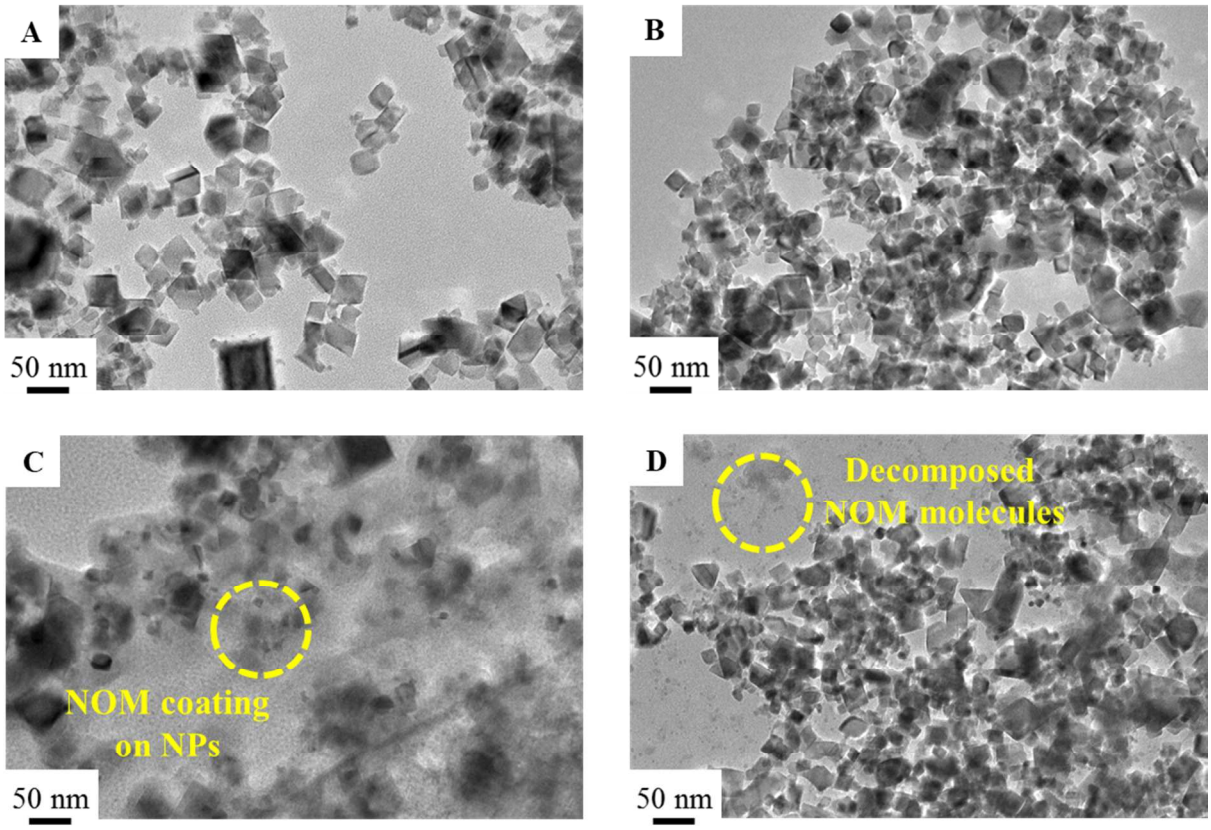
A
50 nm
B
50 nm
C
NOM coating
on NPs
50 nm
D
Decomposed
NOM molecules
50 nm

Fig. 2

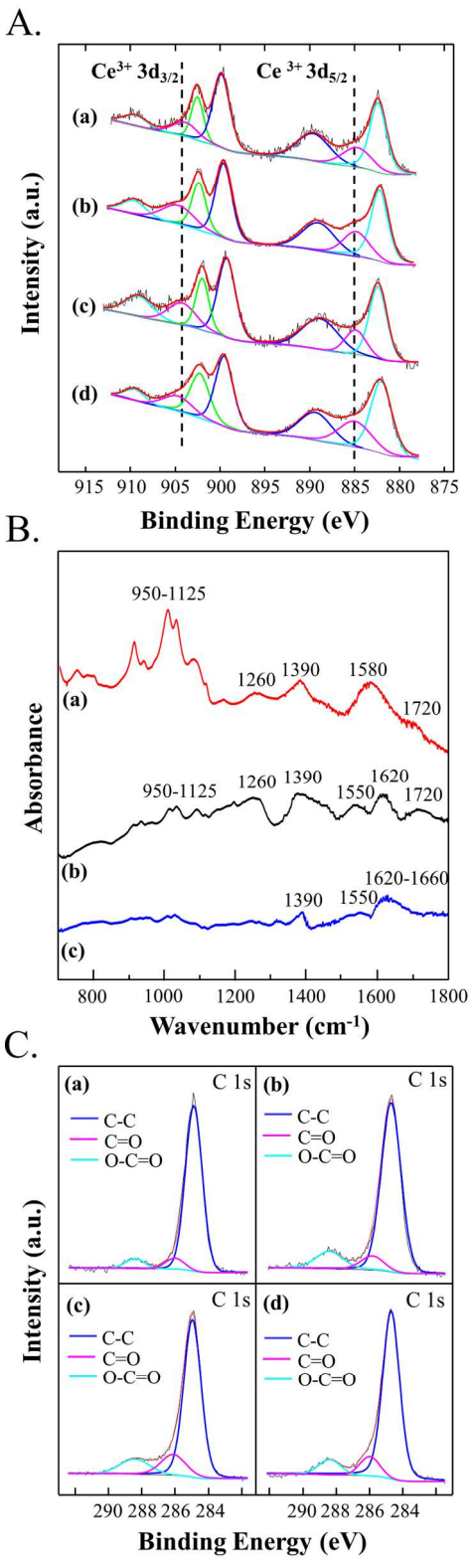
A.
Ce3+ 3d3/2
Ce 3+ 3d5/2
(a)
(b)
(c)
(d)
Intensity (a.u.)
915 910 905 900 895 890 885 880 875
Binding Energy (eV)
B.
950-1125
1260
1390
1580
1720
(a)
950-1125
1260
1390
1550
1620
1720
(b)
1390
1550
1620-1660
(c)
Absorbance
800 1000 1200 1400 1600 1800
Wavenumber (cm-1)
C.
(a)
C 1s
C-C
C=O
O-C=O
(b)
C 1s
C-C
C=O
O-C=O
(c)
C 1s
C-C
C=O
O-C=O
(d)
C 1s
C-C
C=O
O-C=O
Intensity (a.u.)
290 288 286 284
290 288 286 284
Binding Energy (eV)

Fig. 3

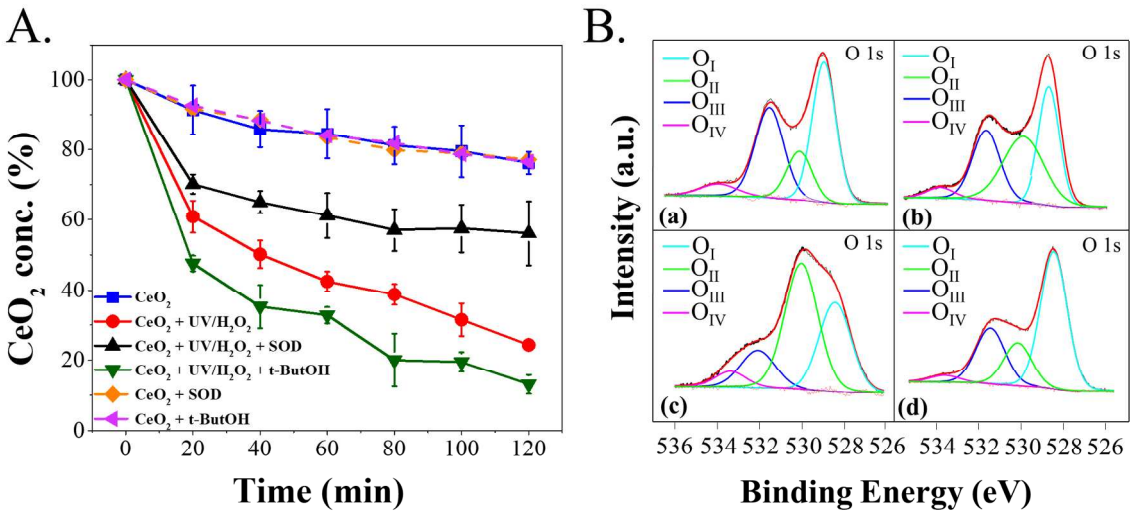
A.
CeO2 conc. (%)
Time (min)
CeO2
CeO2 + UV/H2O2
CeO2 + UV/H2O2 + SOD
CeO2 + UV/H2O2 + t-ButOH
CeO2 + SOD
CeO2 + t-ButOH
B.
Intensity (a.u.)
Binding Energy (eV)
O 1s
OI
OII
OIII
OIV
(a)
(b)
(c)
(d)

Fig. 4

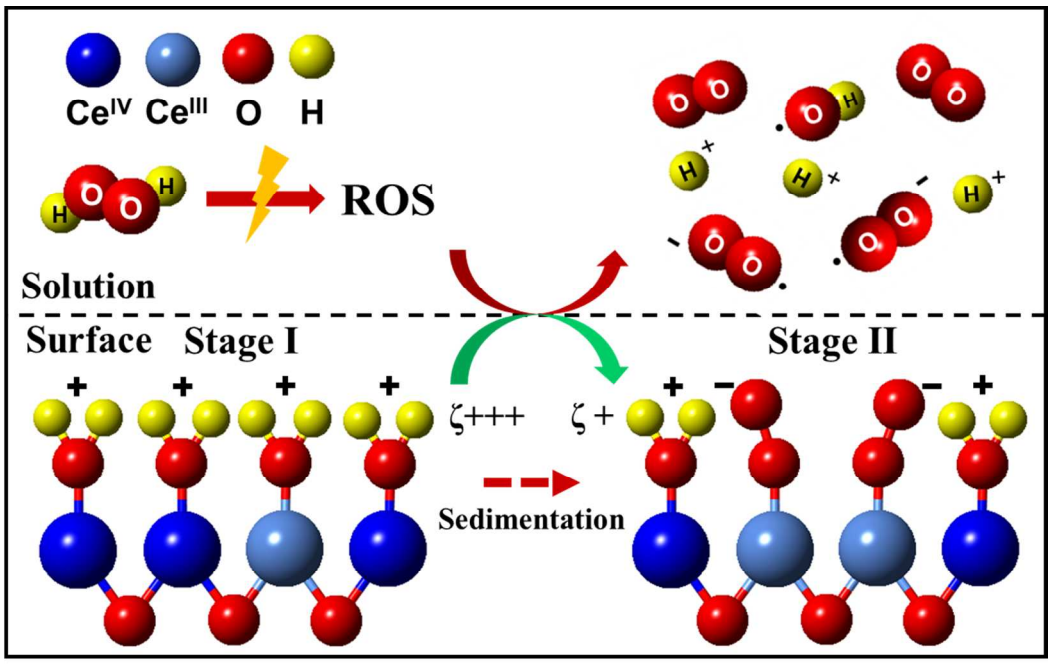
Ce^IV Ce^III O H
ROS
Solution
Surface Stage I
Stage II
ζ+++
ζ +
Sedimentation

Fig. 5

Table of contents entry:

This study delineates the co-effects of UV/H_2O_2 and NOM on the colloidal stability and surface chemical properties of CeO_2 nanoparticles.